Deutsches Zentrum
DLR für Luft- und Raumfahrt

DHBW
Duale Hochschule
Baden-Württemberg

FireF(l)ighter

DLR Design Challenge 2022

Supporting organization:
Duale Hochschule Baden-Württemberg Ravensburg
Campus Friedrichshafen

11.07.2022

Name of supervisor: Prof. Dr.-Ing. Markus Grieb

Head of the student team: Hannah Feiler

List of members of the student team

name	study graduation	number of semesters
Feiler, Hannah	bachelor	4
Loheide, Hannes	bachelor	4
Schaible, Sabrina	bachelor	4
Traber, Maren	bachelor	4
Völkle, Frieder	bachelor	4
Wiegner, Tristan	bachelor	4

Duale Hochschule Baden-Württemberg · Ravensburg
Fallenbrunnen 2, 88045 Friedrichshafen

Prof. Dr.-Ing. Markus Grieb
Lehrprofessor für Luft- und Raum-
fahrtsysteme

DHBW Ravensburg
Campus Friedrichshafen
Fallenbrunnen 2
88045 Friedrichshafen

Telefon + 49.7541.2077-452
Telefax + 49.7541.2077-198

grieb@dhbw-ravensburg.de
www.technik.dhbw-ravensburg.de

01.07.2022

Eigenständigkeitserklärung

Sehr geehrte Damen und Herren,

hiermit bestätige ich, dass die teilnehmenden Studierenden mit dem Thema:

DLR Challenge 2022

selbstständig verfasst und keine anderen als die angegebenen Quellen und Hilfsmittel benutzt haben

Friedrichshafen, den 01.07.2022

Mit freundlichen Grüßen

Prof. Dr.-Ing. Markus Grieb

DHBW Ravensburg
Campus Ravensburg
Marienplatz 2
88212 Ravensburg

Telefon + 49.751.18999-2700
Telefax + 49.751.18999-2701

DHBW Ravensburg
Campus Friedrichshafen
Fallenbrunnen 2
88045 Friedrichshafen

Telefon + 49.7541.2077-0
Telefax + 49.7541.2077-199

info@dhbw-ravensburg.de
www.dhbw-ravensburg.de

Kurzfassung

Die Bedrohung durch verheerende Waldbrände hat in den vergangenen Jahren stark zugenommen. Auch in Mitteleuropa ist der Einsatz durch Flugvehikel zur Brandbekämpfung von Nöten. In dieser Arbeit wurde eine Hubschrauber/Tragschrauber-Konfiguration entwickelt, welche für diese Art Einsätze konzipiert ist. Dabei wird im Folgenden auf den Leistungsbedarf, sowie auf die Wasseraufnahme und -abgabe eingegangen. Zudem beleuchtet diese Ausarbeitung Punkte zur Flugstabilität, wie zum Beispiel die Auslegung des Höhenleitwerks, als auch die Verschiebung des Schwerpunkts während des Fluges. Weiterhin wird ein Flottenkonzept und deren Effizienz vorgestellt, wie auch verschiedene Einsatzszenarien. Bei diversen Berechnungen wird dabei entweder auf die Hubschrauber- oder auf die Tragschrauberkonfiguration Augenmerk gelegt.

Abstract

The threat of devastating forest fires has increased significantly in recent years. Even in Central Europe, the use of air vehicles for firefighting is necessary. In this paper, a helicopter/support helicopter configuration was developed that is designed for this type of operation. In the following, the power requirements as well as the water absorption and release are discussed. In addition, this paper highlights points related to flight stability, such as the design of the tailplane, as well as the shift of the centre of gravity during flight. Furthermore, a fleet concept and its efficiency is presented, as well as various deployment scenarios. In various calculations, attention is paid to either the helicopter or the gyroplane configuration.

Contents

List of figures and tables

List of Figures

List of Tables

Index of symbols

Symbol	Unit	Meaning
G/F	$\frac{N}{m^2}$	disk surface load
A_{rot}	m^2	main rotor area
r_{rot}	m^2	main rotor radius
P	W	power
v	$\frac{m}{s}$	velocity
m	kg	MTOW
g	$\frac{m}{s^2}$	gravity
q	$\frac{rad}{s}$	pitching speed
ρ	$\frac{kg}{m^3}$	density of atmosphere
b_H	m	span of horizontal stabilizer
s_H	m^2	horizontal stabilizer area
$C_{AH\alpha}$		angle-dependent lift coefficient
l_H	m	horizontal stabilizer to Center of Gravity distance
α_H	°	negative angle of attack
Λ		tail extension
C_{AH}		coefficient of lift
A_H	N	lift
M_H	Nm	Moment around Center of Gravity
Ω_R	$\frac{rad}{s}$	angular velocity
t_{Bl}	m	blade depth
K_{Z2}	rad	blade angle
n_{Gl}		glide ratio
n		number of blades

μ_R		advance ratio
C_{WP}		parsitic drag coefficient
S_P	m^2	forehead area
F_G	N	rotor force
n_R	$\frac{U}{min}$	rotor speed
Ω_R	$\frac{rad}{s}$	angular velocity
V	$\frac{m}{s}$	airspeed
$V_B s$	$\frac{m}{s}$	blade tip speed
α_R	rad	rotor pitch angle
β_{Blc}	rad	flapping angle
W_E	N	rotor drag
W_R	N	parasitic drag
C_{ABl0}		zero lift coefficient
AMSL	ft or m or km	Above Mean Sea Level
	ft	feat
NM	nm	nautic miles
kts	nautic miles per hour	knots

1   Introduction

In the last years, the number of forest fires has significantly increased and the extent of the fires has grown too. Though Australia has always been prone to bushfires, the bushfires that occurred during the summer of 2019-20 were an exception in scale and impact on the country. According to estimations 3 billion animals were killed and 74000 km² burned and besides those dramatic impacts, the forest fires promote climate change. In an article from 2021, it is estimated that the bushfires of 2019-20 caused the emission of 715 teragrams of carbon dioxide. [3][4] Even in northern Europe wildfires are becoming more of a problem, in 2018 there was a huge wildfire outbreak in Sweden[5]. Currently, in France 30 fires are reported and have already burned 600 hectares(Cited 11.07.2022)[6].

Though already an urgent issue, a report of the United Nations Environment Programme suggests that the situation will even worsen in the coming decade and century. "Climate change and land-use change are projected to make wildfires more frequent and intense, with a global increase of extreme fires of up to 14 per cent by 2030, 30 per cent by the end of 2050 and 50 per cent by the end of the century, [. . .]". [7] This calls for a new approach and new systems for fighting fires, which are urgent to prevent more incidents that cause human lives and increase economic as well as ecological damage. During the wildfires in California in 2021 drones were being tested by NASA to support the firefighters. Mostly used for thermal imaging and information gathering the drones provided important data to assist the teams and provided relief to the human operators. [8] The given task for the following paper is to develop a system of aircraft working together that should be able to deliver at least 11,000 liters of water to a fire scene in a single firefighting mission. To solve it, it was decided to design a UAV in form of a helicopter that can change into a gyrocopter mode to fly more efficiently and thus fuel-friendly, but without losing the ability to change back into helicopter mode and take off vertically. It was decided to use traditional engines powered by kerosene instead of emission-free electric engines and a remotely piloted aircraft to save weight and enable the aircraft to transport more water at once and easier fulfill the mission requirements which are listed in the tables 1 and 2 below.

Table 1: Mission Requirements

MTOW	5'670 kg
Minimum service height	8'000 ft
EIS	2030
VSTOL-features	
Low noise emissions	

Table 2: Mission Specifications

Distance operational base-fire location	75 nm
Height AMSL operational base	1'000 ft
Height AMSL fire location	2'000 ft
Distance fire location-water source	15 nm
Height AMSL water source	2'000 ft
Temperature	+20°C
Operational area	Europe

The first part of this work constructs the aircraft according to the requirements and specifications mentioned above, whereas the second part evaluates the optimal concept for a fleet of the previously designed aircraft.

2 Sizing and Performance calculation

2.1 General considerations

In the course of designing the performance and the central parameters to be determined for it, the performance-defining flight conditions must first be defined and assigned. This means that depending on the flight condition, either the gyrocopter or the helicopter configuration is used.
In the planned operational scenarios, the aircraft is in cruise or forward flight for by far the longest time, which is why this determines the energy requirement to a large extent. (see also chapter 5)
Since the power requirement is expected to be greatest when the helicopter is hovering, this flight condition is considered to be the defining factor for the design and calculation of the required power. Since most of the parameters between the two configurations overlap and are partly mutually dependent or

even contradictory, an iterative procedure has taken place in the exchange of both design calculations. In the following, the solution from the point of view of the helicopter and in particular its hovering flight is presented and explained.

The essential calculations and required assumptions were performed after [9], [10], [11]. The calculations are based on the basic parameters shown in Table 3. These are derived from the maximum take-off weight in terms of the maximum take-off mass according to requirements and several ratio factors for the predetermination of payload and empty mass according to ([9], chapter 8).

Payload	1417.5kg
MTOW	5670kg
Empty weight	2268kg

Table 3: basic parameters

Furthermore, the atmospheric data are of critical importance, as they significantly influence the efficiency of the rotor and thus the power requirements of the main rotor. Especially the required operation at high altitudes and at high temperatures cause a comparatively low air density. This deviation from the standard atmospheric density at low altitudes must therefore be taken into account. The formulas for determining atmospheric data according to (NASA-TM-X-74335 [12]) provide the data listed in Table 4.

Standard temperature at 8000ft	$-0.85°$C
Standard density at 8000ft	$0.96287\frac{kg}{m^3}$
Actual Temperature (with offset)	$19.15°$C
Actual density (with offset)	$0.89699\frac{kg}{m^3}$

Table 4: atmospheric data

2.2 Helicopter configurations

The design of the main rotor includes not only the radius and thus the blade length, but also the blade depth, speed and number of blades. In the course of this, some considerations based on technical literature are carried out qualitatively.

A first central design parameter for the helicopter configuration is the rotor area. This, in combination

with the hover weight, which is always assumed to be the MTOW for conservative design, determines the circular area load of the rotor. The smaller this load, i.e. the larger the rotor, the lower the power requirement in hover flight. Also, the autorotation characteristics are improved with increasing rotor circular area, which is particularly interesting with regard to the autogyro function. The maximum speed in gyroplane operation, which decreases with increasing rotor blade length, speaks against a too small selected circular area load. More on these calculations can be found in chapter 2.3. Usually the values for this load can be found in the range of $G/F = 100...500N/m2$. ([9], chapter 4).

With a selected disk surface load of $400\frac{N}{m^2}$, the required surface area is about $A_{rot} = 140m^2$ and thus a rotor radius of $r_{rot} = 6.65m$.

An estimate of the rotor power can be made using the flow filament theory by Bernoulli as described in ([11],chapter 2). This is based on simple considerations such as the law of conservation of energy and momentum. They a formula 1 for determining the rotor power. With the hovering performance factor, which is equivalent to an efficiency, another important parameter plays a role in these calculations. This can only be determined exactly in tests or at least simulations. The hovering quality is set somewhat lower in the calculations with $\eta = 0.7$ than would be possible according to the current state of the art [9], because it should be noted that a compromise solution is necessary for the rotor blade geometry with regard to the gyroplane. It can therefore by no means be assumed that the rotor is a specialised hovering rotor.

$$P_{rot,tot} = \frac{1}{\eta} \cdot G \cdot \sqrt{\frac{G}{2 \cdot \rho \cdot A_{rot}}} \tag{1}$$

After the main rotor, the second largest power requirement comes from the torque compensation that is essential. For this purpose, a dual function of two thrust propellers is set up at the side of the fuselage. The double function consists on the one hand of the aforementioned torque compensation and on the other hand of generating the necessary propulsion in gyrocopter mode. From the direction of the necessary compensation, it follows that one propeller must be able to reverse the thrust direction between the two operating cases. For this purpose, a collective blade pitch control is provided.

The power requirement of the pusher propeller when fulfilling the function of the classic tail rotor can be carried out in the same way as for the main rotor. Instead of the weight force, the force that

generates a moment via a lever of 4m is decisive. With a propeller radius of 1m, the power requirement of a thrust propeller in hovering flight is about 195kW.

The torque to be compensated by the main rotor drive is determined by considering head speed and power.

The head speed is another important parameter to be considered, especially with regard to the given noise emission requirements. The blade tip speed should not exceed a value of $v_{bladetip} = 220$ m/s in order to be as quiet as possible ([10], chapter 2.)

The design thus results in a head speed of 300 1/min , which results in a blade tip speed of $v_{bladetip} = 209$ m/s.

In summary, a power of the entire aircraft in fully loaded hovering flight at service ceiling height of about 1.58 MW is to be expected, which has a dimensioning influence on the engine selection. Table 5 summarizes all important performance data and vehicle parameters once again. A useful effect that has

disk surface load	$400\frac{N}{m^2}$
rotor radius	$6.65m$
head speed	$300\frac{1}{min}$
power of rotor and Propellers	$1.58MW$

Table 5: performance data and vehicle parameters

not yet been taken into account is the ground effect, which considerably reduces the power requirement in hover flight near the ground. However, it is very difficult to quantify this effect exactly, but since it can become important in the mission profile with very low hover flights, at least an estimate should be made.

Literature by W. Bittner [9] states that the ground effect occurs at an altitude of twice the rotor radius. According to his formula about the relation between free induced downwind velocity and downwind velocity near to the ground, this would result in a power reduction of 59 kW. However, this figure should be treated with caution, as the planned operation over water is not taken into account in the calculations. Operation over water reduces the ground effect by "yielding", similar to tall grass.

When selecting the number of blades, numerous considerations play a decisive role. First of all, it is generally true that a larger number of blades can reduce noise emissions. On the other hand, however,

there are disadvantages such as an increased complexity of the rotor head or a decrease in efficiency at the same speed, because the blades are increasingly influenced by the wake of the previous blade. [10] In addition to these considerations, vibration effects must be taken into account, which can be examined in detail during a more detailed design phase.

Based on existing prototypes and the criteria described, the vehicle will be equipped with a four-blade rotor. With a typical surface density of 8%, which also yields good results in calculations of gyrocopter operation, the required blade depth is about 0.4m.

Since all the calculations described are based on the 'worst-case' scenario of maximum flight altitude, i.e. minimum density and maximum mass at the same time, it can be stated that the power that will be achieved will be the maximum power. However, this will never be demanded permanently. Also, the power in hovering flight, e.g. due to an empty water or not quite full fuel tank, will usually be significantly below the maximum power. Nevertheless, the maximum power must be used for engine dimensioning.

The engines are dimensioned in such a way that both engines are needed in hover flight, i.e. hover operation with only one engine is not possible.

Due to the significantly reduced performance in gyrocopter operation (see chapter 2.3), this is necessary with only one engine. Thus, there is a re-dundancy which offers a special safety.

In order to meet the requirement of a possible early entry into service, a new development of the engines should not be assumed. Instead, for example, two existing turboshaft turbine engines such as the type "Turbomeca Arriel 2S2", which are already in use in existing helicopters, can be considered for use.

2.3   Gyrocopter configurations

In cruise flight, the gyrodyne should function as a gyrocopter, as it has very good and stable flight characteristics and is more energy efficient. [13]. For the design of a gyroplane, the dimensions of the main rotor are of primary interest. In the previous chapter, the most important geometric dimensions of the rotor have already been determined.

For the power calculation in gyrocopter operation, the radius and blade depth as well as the number of blades are of particular interest. To further design the rotor, the blade profile to be used must also

be selected. A typical airfoil for gyrocopters is the NACA 8-H-12. However, this concept aircraft is a gyrodyne that is also intended to operate in a helicopter configuration. For this reason, this flight condition is important for the airfoil, since helicopter airfoils are often thicker and have a lower glide ratio. Another key reason is that a swashplate with collective pitch is used for flight control. For this reason, the NACA-23015 airfoil, which is also used on helicopters such as the Bell 200 [14], is chosen for a performance estimate. This profile has an average glide ratio of about 80 and a zero lift coefficient of 0.25. Hence, with the parameters, it is even very close to the aforementioned gyroplane profile. [15]

To get an estimation of the dimensions and the performance of such an aircraft, the book "Flugphysik der Tragschrauber" by Holger Duda and Jörg Seewald is used as a reference, in which all performance parameters and specific variables have been calculated using a reference gyrocopter.

The reference gyrocopter used for the calculations is based on the MTOsport, which is produced by the manufacturer Autogyro GmbH. In contrast to the gyrodyne that is to be dimensioned, the reference gyrocopter only has a takeoff mass of just under 400kg, which classifies it as a UL air sports aircraft ([1], p.215). However, the MTOW of this conceptional gyrodyne is to be set at the maximum specified takeoff weight of 5.67t. Another significant difference is the number of rotor blades. The reference flight helicopter has 2 rotor blades. As explained in chapter 2.2, the rotor of the flight helicopter to be dimensioned in this design has a number of blades of 4. The most important reason to choose a rotor with more blades is that the vibration of the rotor gets lower. The rotor, therefore, rotates very smoothly.

In addition, the rotor blades would otherwise become too large, which would make maintenance more difficult. However, it is difficult to make a general statement about this. ([16], S. 129)

2.3.1   Mathmatical Background

Rotorforce

In order to be able to apply the formulas and equations nevertheless, it was assumed that the weight force which the rotor has to carry is distributed equally over 2 two-blade rotors. For this reason, the factor n=1/2 was introduced for the rotor force, since each two-blade rotor only has to bear half of the weight force. Equation: 2 ([1], p.6).

$$F_G = \frac{m \cdot 9.81}{n} \tag{2}$$

Since the required performance in forward flight is of primary interest for the design of the gyrocopter, only the flight condition "forward flight with autorotation" was considered in more detail. This flight condition describes the horizontal straight flight that forms the cruise flight, which exists for most of the flight time and is therefore decisive for a power calculation.

Rotor RPM

In the first step, the rotor speed was calculated as a function of the airspeed in forward flight according to the following equation (see Equation 3).

$$n_R = \sqrt{\frac{F_R}{\rho \cdot t_{Bl} \cdot r^3 \cdot (K_{Z0} + K_{Z1} \cdot \mu_R + K_{Z2} \cdot \mu_R^2)}} \cdot \frac{30}{\pi} \tag{3}$$

The calculation includes parameters of the rotor, such as the blade depth or the radius, as well as the constants K_{Z0}, K_{Z1}, K_{Z2} (see appendix), which are all dependent on the profile properties of the individual rotor blade and its blade pitch angle. With the determined rotor speed, the resulting angular velocity and the advance ratio, the airspeed can be determined by using formula 4. ([1], S. 234)

$$\mu_R = \frac{V}{\Omega_R \cdot r} \tag{4}$$

With the airspeed, all other relevant parameters can be determined via further analytical formulas. ([1], S.68ff.)

Rotor Pitch Angle

The rotor pitch angle is an important quantity, which is required in particular for the calculation of the resistance and therefore for the determination of the power. The following relationship for the calculation is only dependent on rotor parameters and on profile-dependent constants $K_{\alpha\,0}$, $K_{\alpha\,1}$, $K_{\alpha\,2}$. (see eq. 5) ([1], p.71)

$$\alpha_R \approx \frac{t_{Bl}}{r} \cdot \left(K_{\alpha0} + \frac{K_{\alpha2}}{\mu_R^2} \right) + \frac{K_{\alpha1}}{\mu_R^2} \tag{5}$$

Blade Flapping Angle

The flapping angle describes the deflection of a rotor blade from the rotor plane. This deflection is

caused by the fact that the incident flow velocity of a rotor blade varies constantly depending on its current position. The leading blade experiences a much higher incident flow than the returning blade, since the leading blade is additionally influenced by the airspeed. A returning blade runs against the airspeed and generates much less lift than the current leading blade. Consequently, the leading blade is lifted upward out of the rotor plane due to the high lift force, while the trailing blade is deflected downward out of the rotor plane due to the lower lift force. ([1], S.45ff.)

This relationship is extremely important for determining the maximum speed, since the flapping angle increases more and more as the airspeed increases. Consequently, at some point this would reach its limit determined by the design. It could happen that the rotor hits the tail unit or that the occurring forces become too large for the blades and the rotor. For this reason, the flapping angle should not become too large and is limited by a stop. However, the flapping angle can increase during certain maneuvers such as the takeoff run. The takeoff-run does not have to be taken into account, however, as the gyrodyne takes off as a helicopter. [17]

The flapping angle is calculated according to the formula 6. (s. appendix) ([1], S. 70)

$$\beta_{Blc} \approx K_{\beta 0} + K_{\beta 1} * \mu_R \tag{6}$$

Blade Tip Speed

Another important factor is formed by the blade tip speed. This is primarily limited by the leading rotor blade. Its incident flow is considerably higher than that of the trailing blade. If the airspeed is too high, the blade tip speed could exceed Mach 1, which must be avoided. In addition, the rotor should be as quiet as possible, so the blade tip speed should be limited to 220m/s without influence of the airspeed. ([16], p. 124). The blade tip speed can be calculated with formula 7, since both the rotor radius and the angular velocity are known.

$$V_{Bs} = \Omega \cdot r \tag{7}$$

Power

Since the rotor has a certain rotor pitch angle in flight, the lift force does not point vertically upwards. Consequently, a partial component of the lift force points against the direction of flight and thus creates

drag. Formula 8 can be used for a power estimation.

$$W_R = F_G \cdot \sin(\alpha_R) \tag{8}$$

However, only the drag of the rotor has been considered so far. But, the fuselage and all other components of the gyrodyne are also exposed to the airflow and generate drag. To calculate this according to formula 9, the frontal area and the parasitic drag coefficient are required. The face area S_P of the gyrodyne is approximately 2.5 m2 and the drag coefficient C_{WP} was estimated to be 0.8. This value is slightly lower than that of the reference gyrocopter, which can be justified by the fact that the fuselage is more aerodynamically shaped than that of the reference gyrocopter, which has a parasitic drag coefficient of 1.0. This poor value is due to the fact that the cabin is open, which creates way more turbulence.

$$W_P = \frac{\rho}{2} \cdot S_P \cdot V^2 \cdot C_{WP} \tag{9}$$

$$P = (W_R + W_P) \cdot V$$

With the parameters calculated so far, it is now possible to determine whether the rotor with a particular blade profile is suitable for the gyrodyne. ([1], S.107ff.)

2.3.2   Calculation process

To determine whether the rotor designed for the helicopter configuration could also be used in gyroplane operation, the most important parameters had to be determined iteratively. To simplify the calculation, a MATLAB script was written so that not all calculations had to be done by hand. This consists essentially of 2 parts. In the first part, all input parameters are defined, which are needed for the calculations of the mathematical equations listed above. These input parameters and the calculated results are listed in the appendix (tables 7, 8, 9, 10). One calculation was performed for the standard density and one for the lowest density at maximum altitude with maximum temperature deviation. Of particular interest were the maximum speed to be achieved and the power required to hold it.
In order to select the input parameters as suitably as possible, it was examined in each case how the parameters to be entered influence the essential parameters such as power or the blade tip speed. This

influence can also be seen in table 6 (s. appendix). The first line contains the input parameters and the first column contains the calculated parameters, which result from the above relationships from chapter 2. The + means that the calculated parameter increases for increasing the respective input parameter and the - accordingly that the calculated parameter decreases for increasing the input parameter. The color coding indicates whether the respective effect is desired (green) or not (red). However, it still turned out to be very difficult to find the correct parameters for the dimensioning of the rotor and the profile.

Std-Density

The airspeed achieved with the selected parameters is about 73 m/s or 263.2 km/h at a density of 1,225 kg/m$\hat{3}$. The flapping angle is also very low at only 3°. At these conditions, the airspeed is rather limited by the blade tip speed, which is already very high.

Density (8000ft+dt)

However, when the density is very low, the flapping angle increases very much because the blade pitch angle has to be increased. However, a flying speed of 70.1 m/s is still possible, so the flapping angle does not become too large.

Conclusion

The achievable speeds are already in a pretty good range. If the airspeed is to be increased, limiting parameters such as the blade tip speed or the flapping angle, which is currently quite high with a maximum value of 4.6°, increase further. The high flapping angle would have to be limited by a stop at about 8° in order to have a reserve of about 50% as with the reference gyrocopter.[17]

2.3.3   Increased Performance By Attaching a Fixed Wing

Flight Mechanical Effects

By adding wings, both a slight increase in top speed and a reduction in required power can be achieved. In a gyrocopter, the rotor plane must always be inclined backward, so that during horizontal forward flight the rotor is permanently impinged from below and autorotates. However, this means that there is always a partial component of the lift force which is opposite to the direction of flight and therefore

increases the drag. This is not necessary in a fixed-wing aircraft, which is why drag is generally higher in a gyrocopter compared to a classic fixed-wing aircraft. The idea is to lighten the load on the rotor so that the rotor does not have to generate as much lift, since it no longer has to compensate for the entire weight force. This can be achieved by attaching fixed-wings, which compensate for a certain lift component in cruise flight and thus relieve the rotor. However, a functioning autorotation must still be guaranteed. Compared to a conventional gyrocopter, unloading the rotor reduces the angle of attack between the airflow and the rotor plane, which also lowers the rotational speed. Lower rotational speed while maintaining airspeed also results in noise reduction of the gyrodyne. As shown in the tables 8 and 10 (appendix), this value is currently above 220m/s, but can be achieved by installing wings. What remains to be considered is the drag generated by the wings, which is, however, small compared to the savings gained and for this reason is not included in the calculations.

Furthermore, it should be taken into account that the optimization potential depends on the airspeed, since the influence of the rotor drag on the total drag changes. This can be seen in Fig 6 appendix. The proportion of the rotor drag force in the total drag decreases with increasing flight speeds, so that the optimization potential at a flight speed of 70 m/s is only just under 30%.

However, the addition of wings does not only bring advantages. Since they generate a large part of the lift force, moments are also generated which can have a negative influence on the stability of the aircraft. The flapping angle also increases, since the rotor speed decreases due to the unloading, but the blade pitch angle remains constant. Consequently, one solution would be to reduce the blade pitch angle at higher airspeeds when the wings are generating lift. This is also easy to implement in this concept aircraft, since a swashplate with collective and cyclic blade pitch control is used for flight control. [17]

Calculations With Wings

The same MATLAB script was used as in Chapter 2, but the major change was to assume that the wings generate half of the lift in cruise flight and that the blade pitch angle reduced due to the mentioned reasons above. The principle that the wings generate half of the lift in cruise flight was also used in the Fairey Rotodyne. [18] All other input parameters remain unchanged. However, the dimensions of a wing that meets the requirements are still missing. To keep the induced drag as low as

possible, a wing with a relatively high aspect ratio should be selected. However, this should not be too high for reasons of stiffness, since the gyrodyne generates a strong downwash in helicopter operation. Accordingly, the drag created by the wings is also not known and is not taken into account for the calculations. The results can be found in the appendix. [17]

Std-Density

If the blade pitch angle is set to -0.2°, the rotor speed can be limited to 220 rpm. However, the speed would drop to 66.1 m/s. The power savings, however, would also be very considerable, at around 33%.

Density (8000ft+dT)

If the blade pitch angle is reduced to 0.9°, the rotor speed can be reduced to 220 m/s without any major loss of speed. The energy saving would be about 32 %.

Conclusion

The calculation shows that the power can be greatly reduced. However, the influence of the drag created by the airfoils was neglected, which is why the resulting savings are probably lower. Nevertheless, the influence of the induced drag of the wings on the total drag is rather uncritical, which is why it is not considered for the calculations. Due to the low blade pitch angle, the flapping angle also drops in this simulation. However, a more accurate program would be needed to verify the results.

3   Flight stability and design of the horizontal stabilizer

According to the design concept, the flying object should function as a helicopter during takeoff and landing. Other flight phases are performed as a gyrocopter. Since control in helicopter operations is provided by the swashplate, tailplanes, or rather the horizontal stabilizer, are only relevant for flight stability in forward flight. Flight stability and the associated dimensioning of the horizontal stabilizer will be the subject of this chapter. The basic calculations and information are mainly taken from the book "Flugphysik der Tragschrauber. Verstehen und Berechnen" by Holger Duda and Jörg Seewald, published by Springer Verlag in 2016 [1]. In the calculation examples listed there, reference gyrocopters are used which have significantly smaller dimensions than the one designed here. Since there are hardly any gyroplanes of this size category in reality, it was not possible to determine corresponding values

with which the horizontal stabilizer could be calculated for the gyroplane here. Wind tunnel tests would be necessary to create the corresponding calculation basis. Therefore, it is only presented here how a calculation with suitable reference values could be carried out, and what has to be taken into account for flight stability in general.

In general, flight stability means that the gyroplane returns to its original position independently after a disturbance. This can take the form of oscillations around this initial position. However, flight stability also means that these oscillations are damped accordingly so that they result in this initial position after a limited time. In the specific case of the horizontal stabilizer of the gyroplane, it means that a disturbance occurs which triggers a pitching movement upwards or downwards, which must be compensated. In this case, we assume that the nose of the gyroplane is pitching upwards from below due to a gust. The reverse case is also possible, of course, but this is not considered separately due to the mirror image.

Depending on the speed of the flying object, the external conditions and the design of the horizontal stabilizer, the flying object is now able to compensate this disturbance more or less well. In general, the larger the tailplane, the better the flight stability. In theory, the tailplane can be enormously large in order to compensate for the disturbance as well as possible, but in practice this fails due to the fact that a tailplane is also linked to weight and size specifications that can be implemented within the framework of the flying object.[16]

Flight stability is achieved by the horizontal stabilizer as follows: Unlike the rotor or the wings of an aircraft, the horizontal stabilizer has a negative angle of attack, which generates downforce accordingly. However, if the gyroplane now pitches up due to the disturbance, the elevator suddenly generates lift at the rear of the gyroplane due to the changed angle, i.e. a stabilizing downward pitching moment around the center of gravity. The horizontal stabilizer counteracts the disturbance, what is also shown in Fig. 1.[1] In order to generate the stabilizing moment equilibrium, the lift of the rotor behind the center of gravity of the gyroplane must also act to generate a corresponding counter moment to the disturbance. However, since the case here is a hybrid gyroplane/helicopter solution, the center of gravity should not be too far ahead of the point of application of the rotor lift, as this can have a destabilizing effect in helicopter operation. Helicopters are fundamentally unstable, which would have to be taken into account in this case.
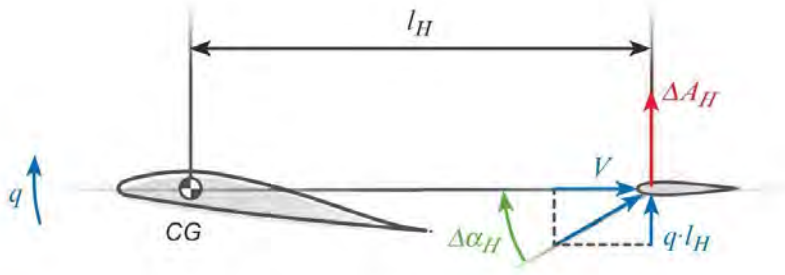
Figure 1: Wing and Horizontal Stabilizer ([1], S. 152)

The following calculations [1] should now be made to design the horizontal stabilizer. If the concept described here is continued, the variables used should be replaced by experimentally determined values in order to be able to qualitatively dimension the tailplane.

A pitching-up disturbance is assumed, which triggers a pitching speed q of the gyroplane. The gyroplane flies at a speed v. The horizontal stabilizer is at a horizontal distance lH from the center of gravity. The change of the angle of attack results from this with:

$$\Delta\alpha_{\mathrm{H}} = \arctan\frac{q \cdot l_H}{v} \approx \frac{q \cdot l_H}{v} \tag{10}$$

The approximation is valid for small angles. With a vertical stabilizer of span b_H and area $S_{\mathrm{H'}}$, the lift coefficient can be calculated via the aspect ratio Λ using the extended load line theory (12).

$$\Lambda = \frac{b_H^2}{S_H} \tag{11}$$

$$C_{AH\alpha} = \frac{2 \cdot \pi \cdot \Lambda}{2 + \sqrt{\Lambda^2 + 4}} \tag{12}$$

$$C_{AH} = C_{AH\alpha} \cdot \Delta\alpha_H \tag{13}$$

(10), (12) and (13) in (14) give the lift change ΔA (15) generated by the horizontal stabilizer and the resulting counteracting moment M (16):

$$\Delta A_H = \frac{\rho}{2} \cdot v^2 \cdot s_H \cdot C_{AH} \tag{14}$$

$$\Delta A_H = \frac{\rho}{2} \cdot v^2 \cdot s_H \cdot C_{AH\alpha} \cdot \frac{q \cdot l_H}{v} \tag{15}$$

$$\Delta M = -\frac{\rho}{2} \cdot s_H \cdot L_H^2 \cdot v \cdot q \cdot C_{AH\alpha} \tag{16}$$

To achieve appropriate flight stability, the resulting moments of the horizontal stabilizer, rotor and propeller must lead to a moment equilibrium. For this purpose, the horizontal stabilizer must be designed experimentally in order to determine reference values for the calculation.

For the calculations presented here, the extended load line theory was used, which is verified as follows: The extended load line theory applies to an elliptical lift distribution at the stabilizer, which is presented here as shown in Figure 2. In the y-direction, the lift is plotted against the tail length in the x-direction. The lift distribution at the empennage is elliptical.
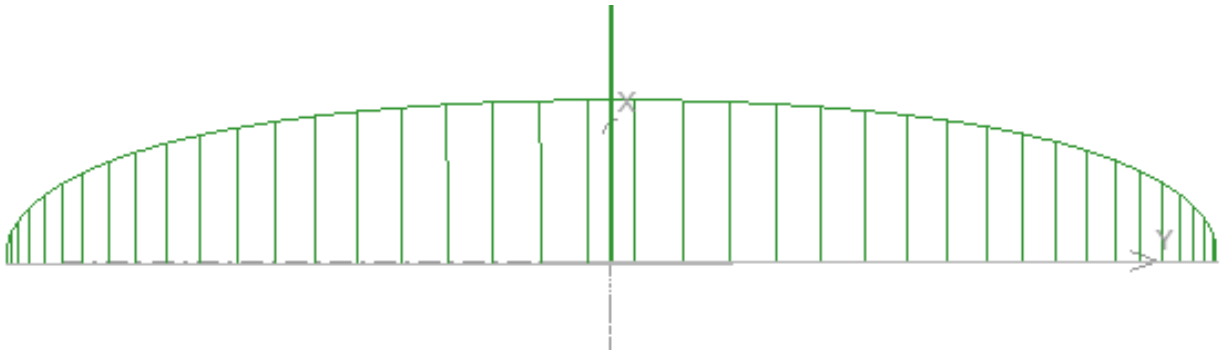

Figure 2: Lift Distribution on the Horizontal Stabilizer [2]

For the verification, we first assume a tail unit without end plates. Figure 3 shows for this case in blue the resulting pitching moment at different angles of attack alpha for three different calculation methods. Shown is the extended load line theory (noEnd erw. Theorie), a vortex lattice method (VLM2_noEnd) and the CFD simulation(noEnd_CFD).

As can be seen from the three blue graphs, the pitching moment is almost the same for all three methods for small angles of attack. The extended contact line theory is verified for the calculation of the lift through the stabilizer. At higher angles of attack, the results of the individual methods deviate further from each other, which is related to the separation but is not important in our calculations with small angles of attack.

Furthermore, two other cases are shown in Figure 3 by the three different methods. the green graphs show the results for a stabilizer with small end discs and the red graph for a stabilizer with larger end
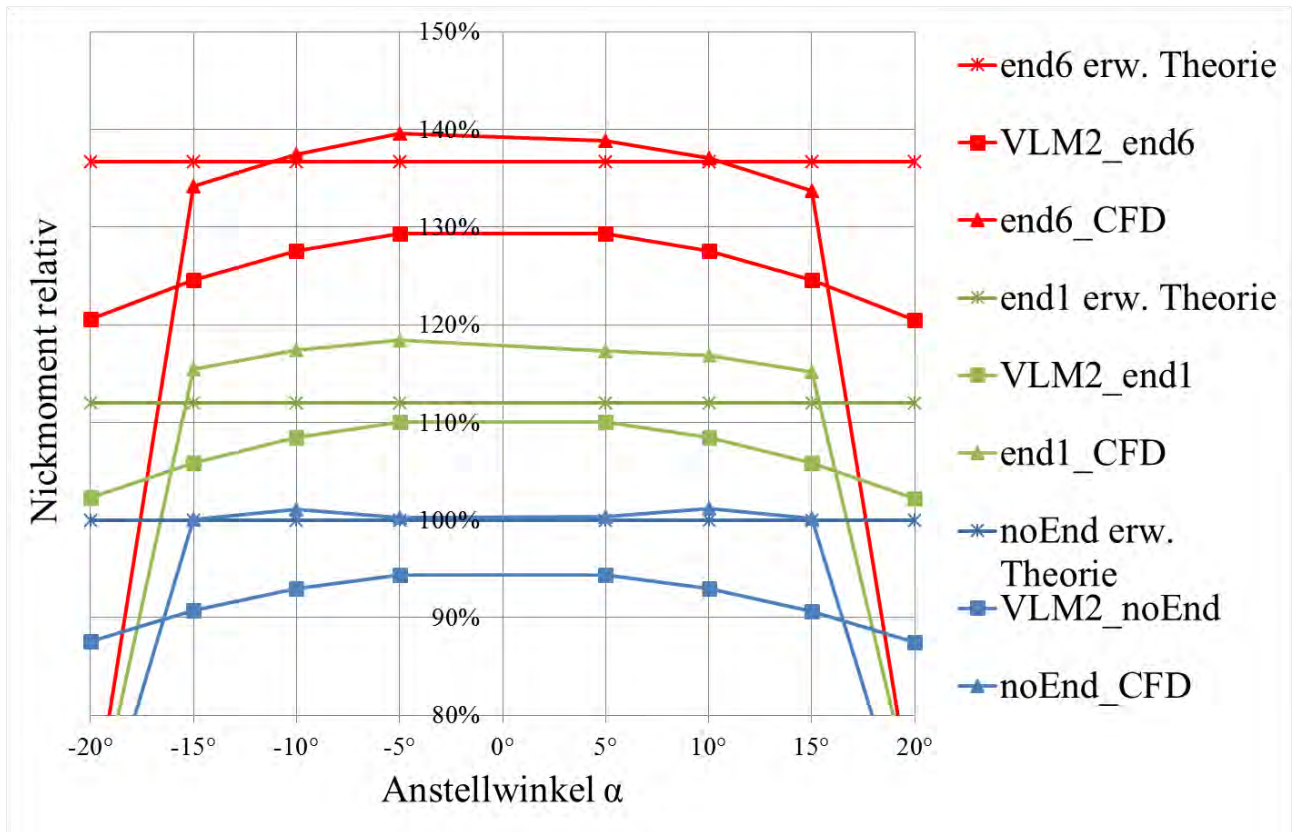
Figure 3: Verification of Different Methods [2]

discs. It can be seen that the use of end discs increases the lift on the empennage and thus its effect. It would therefore also be possible to achieve corresponding moments for smaller tail surfaces with larger end discs. This is because the end plates make it difficult to equalize pressure at the outer edges. That optimization option should definitely be taken into account when designing the tailplane.[2]

Relevant for the stabilizing moment is not only the tailplane area but also the lever arm, which depends on the position of the center of gravity. Since in this case a loading by water takes place, the center of gravity and thus also the lever arm can change in the course. In this case, however, the gyroplane should be designed in such a way that the water tank is located directly in the center under the center of gravity of the gyroplane. This means that the overall center of gravity only changes accordingly in the z-direction upwards or downwards during loading and unloading. However, the distance to the horizontal stabilizer and thus the lever arm remains constant. The exact course of the center of gravity position is shown in Figure 4.
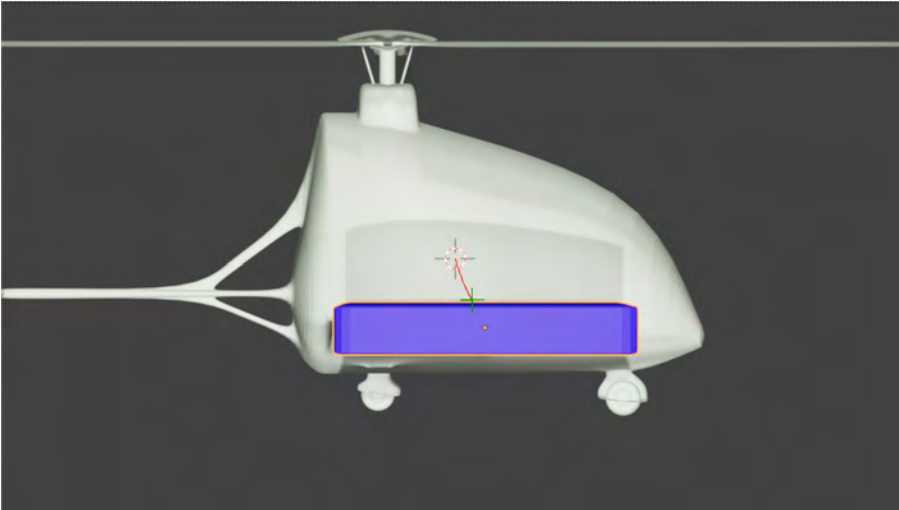
Figure 4: Center of gravity shift

4   Motorization

If the gyrodyne is operated in the helicopter configuration, the main rotor must be actively driven, which also requires torque compensation. In gyrocopter operation, on the other hand, the rotor no longer needs to be driven. Instead, a certain amount of propulsion is now required to compensate for the drag of the gyrodyne. For this reason, it was decided that a propeller would be mounted at each end of the wing. The turbines that drive the two propellers and the rotor, on the other hand, are located at the wing root, so that the wings can be built lightweight, since the weight of the turbine is absent. The corresponding considerations for the necessary power can be found in chapter 2.2, since the required power for helicopter operation is much higher than for gyrocopter operation.

To keep the design as simple as possible, the turbines run at a constant speed, so that only the blade angle for the two propellers can be adjusted to influence the generated thrust. This way, there is also no influence if the rotor is to be kept at constant speed, but the propellers turn asynchronously.

5   Water intake and delivery system

To get water into our flying vehicle, we use the function of a wet vacuum cleaner. The special thing about a wet vacuum cleaner is that the particles sucked in do not pass through the motor, as this would cause a short circuit. It is possible to suck in both wet and dry particles with the principle of the wet-dry vacuum cleaner. This allows us to use our vehicle in a wide range of applications. The

Hydra Red mud and dirt vacuum cleaner from HELPI [19] is used for this purpose. With the help of the suction function, the extinguishing water is sucked into the container. When the container fills up, the device automatically switches on its pumping function. This is advantageous, as a conventional float switch can be extremely error-prone. The pumped-off water is fed by the dirty water pump into another large tank where it is stored. With a suction capacity of 15000 litres per hour, the water is transferred from the small tank to the large one. The stainless steel dirty water pump has the capacity to suck in 24 m³ of water per hour with a grain diameter of up to 45mm. This makes it possible to take in muddy or contaminated water. The total weight of this unit is 33 kg. The suction hose is 12m long, but can be extended as required. In general, the unit works quite quietly at 64 dB. Another advantage is that the unit can be operated at 220 V. The cost of the vacuum cleaner, including VAT, is about 3250 euros.

The tank for storing the water is made of stainless steel V4A with a steel grade of 1.440. This steel weighs 8kg per m² with a thickness of 1mm. The thickness of the tank wall is set at 1.5 mm, so that an area of 8m² with this thickness results in a weight of 96 kg. Our tank can now hold and store up to 1500 litres of water. The price of the steel is between 10 and 12 euros per kilogram. Therefore, the cost of the steel tank is around 960-1152 euros.

Despite the fact that the pump takes 3.75 minutes to fill the tank, this option has the advantage that it is integrated directly into the fuselage of the vehicle. Furthermore, due to the large diameter of the suction hose, there are hardly any restrictions as far as the degree of contamination is concerned.

Another alternative that would be possible for this aircraft would be a conventional extinguishing bag. This is an option that could possibly also be provided for some flying vehicles to relieve the time factor of water intake. However, the disadvantage here is that the aircraft must fly as far as possible to the water body. In the configuration with a suction cup and a hose, it is possible to reach the water from a greater distance. This is not only beneficial for the aircraft and its protection on the propellers and other vulnerable parts. It also allows access to small overgrown pools that cannot be used with a conventional vehicle.

6   Operational Fleet Concept

The aerial firefighting fleet consists of 10 aircraft. The water tank of each aerial firefighting vehicle has a volume of 1.5 m^3 and can thus hold 1,500 kg of water. In total, the whole fleet can carry 15,000 kg of water for each firefighting attack. The fuel tank holds 800 kg of kerosene when fully filled. The energy density of kerosene is 11.9 kWh/kg. Taking this into consideration, the total energy available to the system is 9520 kWh. The emergency fuel reserve holds fuel for a flight of at least 30min in gyro mode according to the recommendation of the German Federal Aviation Authority. Accordingly, 70 kg of the 800 kg of fuel carried are conservatively declared as emergency reserve. The emergency reserve should only be used in critical situations. In addition, 5% more fuel than calculated should be carried to compensate for possible increased consumption due to external conditions, such as headwinds. The efficiency of shaft engines is assumed to be $\eta = 0.4$.

6.1   Standard Mission

	Mode of operation [-]	Water tank [-]	Duration [h]	Power [kW]	Energy [kWh]	Fuel consumed [kg]
1. Take-off	Helicopter	full	0.10	3942	394.2	33.1
2. Flight from the base to the fire scene	Gyrocopter	full	0.46	1750	805.0	67.6
3. Fire-fighting operation	Gyrocopter	full -> empty	negligible	1750	negligible	negligible
4. Flight from the fire scene to the water source	Gyrocopter	empty	0.09	1525	137.6	11.6
5. Water uptake	Helicopter	empty -> full	0.07	3456	241.9	20.3
6. Flight from the water source to the fire scene	Gyrocopter	full	0.09	1750	158.0	13.3
7. Firefighting operation	Gyrocopter	full -> empty	negligible	1750	negligible	negligible
8. Flight from the fire scene to the base	Gyrocopter	empty	0.46	1525	701.5	58.9
9. Landing	Helicopter	empty	0.10	2968	296.8	24.9
Total *			3.87		8110.0	681.7

* with eleven repetitions of steps 4., 5., 6., 7.

Figure 5: Standard Mission

The firefighting mission is divided into different flight phases, during which the required power, the mode of operation and the fuel consumption differ. Figure 5 gives an overview of the mission parameters of the standard mission. The firefighting mission is divided into different flight phases, during which the required power also differs. Figure 5 gives an overview of the mission parameters of the standard mission. The power required during the water drop is considered negligible, since the water drop in the overflight takes only a few seconds and sufficient reserve has been included in the calculation anyway. The fleet departs from the airport for the initial firefighting attack with the fuel tank filled. Ideally, the water tank should be filled with 1,500kg of water by all fleet members at the base, since the energy

requirement is lower when flying directly from the airport to the fire scene without making a detour to the water source to fill the water tank beforehand. The water intake by using the wet aspirator is designed in such a way that even water sources that are forested all around can be used from a safe distance.

Taking into account the 5% increase in consumption, the water source can be approached a total of eleven times during the mission. Only then does one have to return to the base at the airport to refuel. In terms of time, the fuel will last for more than 3h 45min. Since it can be assumed that the pilot also needs a break or must be relieved by a colleague, the return to the base is necessary at this point anyway. After 15min, which are needed to refill the fuel and water tanks, the fleet is ready for action again. This concept can be followed continuously for the full 24h.

6.2   Mission Variations

6.2.1   Influence of the water tank on the energy consumption

As already mentioned, despite the higher weight, it is more efficient to start from the base with a filled water tank, since this saves the detour via the water source. In the worst case, according to the task definition, it must be assumed that in this case an additional distance of 30NM must be covered. In some circumstances, it may still make sense for a few of the aircraft to take off with empty water tanks and fill them at the water source 15 NM away from the fire scene. If the water source is relatively small, it can be assumed that not all aircraft can take up water at the same time. Therefore, staggering the water intake is more efficient. Since no precise indication of the size of the water source is given, this is a purely qualitative consideration and it must be decided for each mission on a case-by-case basis whether it makes sense to allow a certain number of aircraft to take off empty. In addition, a split fleet can ensure a continuous firefighting attack over a longer period of time. Furthermore, fewer aircraft are then in a confined space, which improves the safety of mission participants. A comparison of the mission parameters for the time between takeoff and reaching the fire site is shown in Figure 6 for the two cases takeoff with full tank and direct route to the airport and takeoff with empty water tank and detour via the water source.

Number of		Average energy required per aircraft [kWh]	Average fuel consumption per aircraft [kg]	Total required energy [kWh]	Total required fuel [kg]
Aircraft (full water tank*)	Aircraft (empty water tank**)				
10	0	1200.0	100.7	12000	1007
7	3	1301.2	117.6	13012	1176
5	5	1368.7	118.9	13687	1189
0	10	1537.4	137.1	15374	1370

* Aircraft takes off with full water tank and flies directly to the fire scene
** Aircraft takes off with empty water tank and flies first to the water source and then to the fire scene

Figure 6: Mission Variations

6.2.2   Cooperation with ground staff

In particular, cooperation with the ground crew is essential for fighting forest fires. Although large-scale forest fires can only be fought from the air, small ground fires, in which mainly the vegetation near the ground is affected by the fire, can also be brought under control by ground troops. If the fire grows larger or the danger of forest fires increases, the airborne firefighters should be informed in good time so that they can take all the necessary precautions and fill the water tanks of the aircraft. Further spread of the forest fire can also be prevented by supporting the ground forces, for example by laying a fire-retardant foam carpet. In addition, ground forces can contain newly emerging fires through flying sparks and extinguish pockets of fire with fire patches.

6.2.3   Inland Scenario in Europe

Due to climate change, countries in southern Europe, such as Portugal, Spain, Greece and Italy, are more frequently affected by droughts and heat waves, as is currently the case. This leads to an increased risk of forest fires in the affected regions. The droughts are also causing many reservoirs, smaller rivers and ponds to dry out. Due to this, an alternative strategy must be developed in the inland scenario (for example, in the Spanish Inland), as it cannot be assumed that a water resource that can be used to refill the water tank during the firefighting mission will be available within a reasonable distance from the fire scene.

A very common method that increases the extinguishing effect is to add additives to the extinguishing agent, such as phosphates, which act as fire retardants, and thickeners, which ensure that the extinguishing agent sticks to the trees longer. It is also possible to use flame retardants based on ammonium polyphosphate. The disadvantage of most flame retardants is that they are harmful to the environment and often form toxic fire gases. It would therefore be important to use a flame retardant

that is not harmful to the environment. In any case, it would be desirable to use an environmentally friendly extinguishing agent. With people's increasing environmental awareness, many advances have been made in the field in recent years.

6.2.4   Coastal Scenario

Sufficient water is available on the coast for fire-fighting purposes and the mission can usually be carried out according to standard mission. However, the salt water has a negative impact on the environment. The salt water is absorbed by the plants and gets into the soil. If a freshwater source is also available, this should be preferred.

6.2.5   Secondary functions

In addition, it is possible to operate this vehicle in other ways. For example, if a region is affected by severe flooding, the aircraft can remedy the situation by helping to pump out certain areas. Due to the large diameter of the suction and extraction hoses, it is also possible, for example, to fill flat roofs with gravel or to carry out other roof planting. In addition, the lift/carry configuration can be used as a means of transport in the future to carry various pieces of luggage.
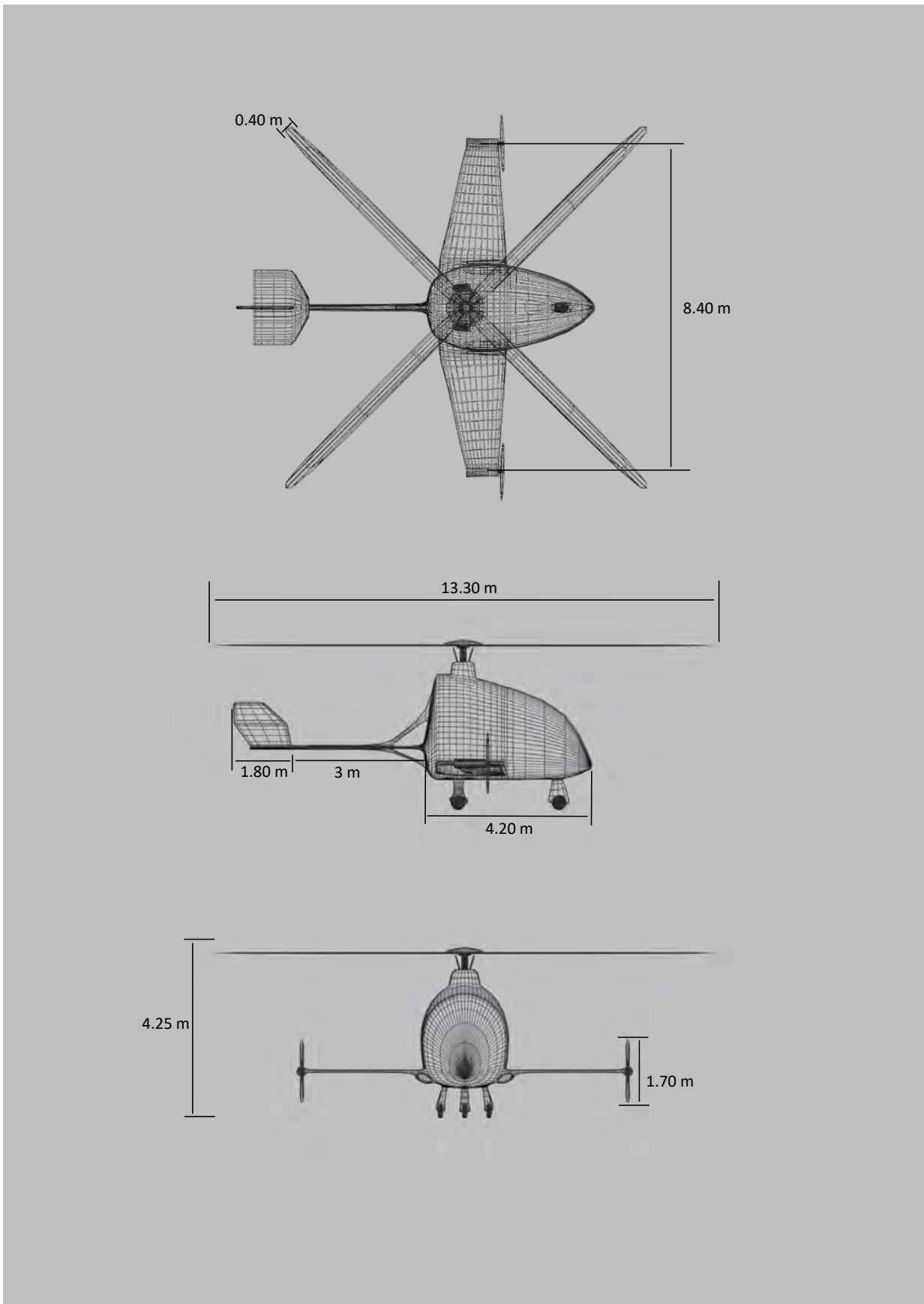
7   Three-side view of the vehicle

Figure 7: Three-side view

8   Conclusion

All in all, this configuration of a helicopter or a gyroplane has been tested for the first time with regard to its flight stability and its power requirements. By means of further testing in, for example, a wind tunnel, the values can be verified. This is only the initial proposal. With further tests and more precise calculations, it is possible that the ideas already highlighted here will be modified or even replaced. However, in this elaboration, assumptions of all important parameters, such as water absorption and the dimensioning of the entire vehicle, have been made for the first time. With these, the exact elaboration of this vehicle can now begin in the next work step. The fleet concept was also thought through to enable the greatest possible water absorption and release within 24 hours efficiently and quickly. The concept of our FireF(l)ighter was thought through and rounded off with further operational scenarios.

References

[1] DUDA, HOLGER; SEEWALD, JÖRG: Flugphysik der Tragschrauber. Verstehen und Berechnen.; Springer Verlag; Berlin, Heidelberg, 2016

[2] VÖLKLE, FRIEDER: Studienarbeit; Entwurf einer Leitwerkskonfiguration für einen neusartigen Multikopter unter Berücksichtigung von Rotorinteraktionen; Donauwörth, 2022

[3] IVAR R. VAN DER VELDE ET ALII.: Vast CO2 release from Australian fires in 2019-2020 constrained by satellite, Adress: https://doi.org/10.1038/s41586-021-03712-y, published online: 15 September 2021

[4] WWF: WWF Report: Australia's 2019-2020 Bushfires: the wildlife toll, 2020

[5] PATEL, KASHA: Scarcely Seen Scandinavian Fires (nasa.gov), July 21,2018

[6] DYLLA CAROLIN: Waldbrände in Frankreich: Dutzende Feuer gleichzeitig; Tagesschau, o.J.

[7] UNEP: Number of wildfires to rise by 50% by 2100 and governments are not prepared, experts warn, UNEP Press Release, o.J.

[8] TABOR, ABBY: At California Blazes, NASA Team Observes How Drones Fight Wildfire, NASA, NASA's Ames Research Center, Last updated: October 19, 2021

[9] BITTNER, WALTER: Flugmechanik der Hubschrauber: Technologie, das Flugdynamische System Hubschrauber, Flugstabilitäten, Steuerbarkeit; Springer Verlag, 4. Auflage; Berlin, Heidelberg, 2014

[10] VAN DER WALL, BEREND GERDES: Grundlagen der Dynamik von Hubschrauber-Rotoren; Springer Vieweg; Berlin, 2018

[11] VAN DER WALL, BEREND GERDES: Grundlagen der Hubschrauber-Aerodynamik; Springer Verlag GmbH, 2. Auflage; Berlin, Heidelberg, 2020

[12] NATIONAL OCEANIC AND ATMOSPHERIC ADMINISTRATION; NATIONAL AERONAUTICS AND SPACE ADMINISTRATION; UNITED STATES AIR FORCE: U.S. Standard Atmosphere,1976, Washington DC (USA), October 1976

[13] FLIEGMITUNS: Gyrocopter - Hubschrauber oder Flugzeug; Adress: https://www.fliegmituns.de/gyrocopter-tragschrauber/tragschrauber-gyrocopter-technik

[14] ENG TIPS: What airfoils are used in Helicopter Main Rotors?, Adress: https://www.eng-tips.com/faqs.cfm?fid=645, 2003

[15] AIRFOIL TOOLS: NACA 23015; Adress: http://airfoiltools.com/airfoil/details?airfoil=naca23015-il#polars , 2022

[16] BITTNER, WALTER: Flugmechanik der Hubschrauber: Technologie, das Flugdynamische System Hubschrauber, Flugstabilitäten, Steuerbarkeiten; Springer Verlag; Berlin, Heidelberg, 2009

[17] SACHS, DUDA, SEEWALD: Leistungssteigerung von Tragschraubern durch Starrflügler: DLR Institut für Flugsystemtechnik, Braunschweig, 2014

[18] LAITIMES: A black-tech Fairey Rotodyne aircraft that combines rotorcraft, helicopters and fixed-wing aircraft; Adress:https://www.laitimes.com/en/article/3l4ok_41tp8.html

[19] HELPI: Schlamm- & Schmutzwassersauger Hydra Red: Der Feuerwehr Wassersauger; Adress: https://helpishop.de/

[20] CARTER AVIATION TECHNOLOGIES: Carter SRC Technology Primer, Adress: http://carteraero.com/files/Carter_Brochure_Carter_SRC_Technology.pdf

Appendix

A: Pictures of the vehicle

B: Constants for mathmatical calculations

$$K_{wBl} \approx \frac{1}{6 \cdot \pi} \bullet \left[\frac{2 \cdot \pi}{n_{Gl}} - \left(C_{ABl0} + 2 \cdot \pi \cdot \varepsilon_{Bl} \right) \bullet \sqrt{(C_{ABl0} + 2 \cdot pi \cdot \varepsilon_{Bl}) \cdot \left(\left(C_{ABl0} + 2 \cdot \pi \cdot \varepsilon_{Bl} \right) + \frac{5 \cdot \pi}{n_{Gl}} \right) + \left(\frac{2 \cdot \pi}{n_{Gl}} \right)^2} \right] \bullet$$

$$KZ0K_{Z0} \approx \left[\pi \cdot K_{wBl} + \frac{1}{3} \bullet \left(2 \cdot \pi \cdot \varepsilon_{Bl} + C_{ABl0} \right) \right]$$

$$K_{Z0} \approx - \pi \cdot K_{\beta 0}$$

$$K_{\beta} \approx 2 \cdot \left[\frac{2}{3 \cdot \pi} \cdot (C_{ABl0} + 2 \cdot pi \cdot \varepsilon_{Bl}) + K_{wBl} \right]$$

Linear Regression:

$$\beta_{Blc} = \frac{\mu_R}{1+2\cdot\mu_R^2} \cdot K_\beta \approx K_{\beta 0} + K_{\beta 1}\cdot\mu_R$$

$$K_{\beta 0} \approx 0.025\cdot K_\beta$$

$$K_{\beta 1} \approx 0.78 \cdot K_\beta$$

$$K_{Z1} \approx -\pi\cdot K_{\beta 0}$$

$$K_{Z2} \approx \frac{C_{ABl0}+2\cdot\pi\cdot\varepsilon_{Bl}}{2} - \pi\cdot K_{\beta 1}$$

$$K_{z0} \approx \left[\pi\cdot K_{wBl} + \frac{1}{3}\cdot\left(2\cdot\pi\cdot\varepsilon_{Bl} + A_{Bl0}\right)\right]$$

$$K_{\alpha 0} \approx \frac{K_{wRi}\cdot K_{Z2}}{\pi}$$

$$K_{\alpha 1} \approx \frac{K_{wRi}\cdot K_{Z2}}{\pi} \cdot \frac{r}{t_{Bl}} + K_{wBl}$$

$$K_{\alpha 0} \approx \frac{K_{wRi}\cdot K_{Z0}}{\pi}$$

C: Appendix for chapter 2.3

Outlook/Evaluation Of The Gyrodyne Concept

The achieved airspeed of 70m/s seems relatively low in contrast to other similar projects. The company "Carter Aviation", for example, promises speeds of up to 450kts without the leading blade exceeding a speed of Mach 0.95. This is achieved by reducing the blade pitch angle of the rotor blades so that the rotor accounts for only 10% of the total drag. In addition, the rotor has an advance ratio > 1 in cruise flight, which has never been seen before on any aircraft. This would mean that the returning rotor blade would experiences an entirely reversed flow. [20]

However, this could not be considered with the calculation methods used in this document. For a more profound calculation, however, this consideration of combining the characteristics of a fixed-wing aircraft and a helicopter would be quite reasonable because of the energy savings and the high speeds.

Transition Helicopter and Gyrocopter Configuration

The appendix contains the "Transition" figure. In this, the total drag in gyrocopter operation without consideration of the wings is plotted against the airspeed. There is a clearly recognizable minimum at a certain speed. The diagram can be divided into 2 sections based on this specific speed. If the speed of the gyrodyne is greater than the limiting one, the gyrocopter is on the front side of the performance curve. If it is lower, it is on the back side of the curve. On the back side, however, the flight behaviour is completely different from the usual flight characteristics of a gyrocopter. The diagram was created with an air density at 8000ft with maximum temperature deviation to cover the worst case. For higher densities the limiting speed would be much lower.

On the front side of the curve, lifting the nose causes the gyrocopter to slow down and reduce drag and the gyroplane begins to climb. On the reverse side of the power curve, raising the nose leads to a rapid increase in drag. Consequently, the gyroplane now enters a descent. ([1], p. 113)

It would make sense to transition to helicopter mode at the critical speed of about 50 m/s for the reasons mentioned above.

D: Tables and Figures for chapter 2.3

Für große Werte	Zero lift coefficient	Blade angle	Glide ratio	Blade depth
Leistung	-	-	+	-
Schlagwinkel	-	-	-	Const.
Blattspitzengeschw.	-	-	+	-
Fluggeschwindigkeit	-	-	-	-

Table 6: input parameters and effects

Calculations without wings

Std density:

Rotor radius [m]	6.65
Blade depth [m]	0.4
Number of blades	4
Zero lift coefficient	0.25
Blade angle [°]	1.7
Glide ratio	80
Density [kg/m^3]	1.225 for Std
Advance ratio	0.3

Table 7: Calc. without wings: Std: inputs

power [kW]	1372.1
flapping angle [°]	2.04
blade tip speed [m/s]	243.5
speed [m/s]	73.1

Table 8: Calc. without wings: Std: results

Density (8000ft+dT):

Rotor radius [m]	6.65
Blade depth [m]	0.4
Number of blades	4
Zero lift coefficient	0.25
Blade angle [°]	4
Glide ratio	80
Density [kg/m^3]	0.86966 for 8000ft + dT
Advance ratio	0.3

Table 9: Calc. without wings: density: inputs

power [kW]	999.6
flapping angle [°]	4.6
blade tip speed [m/s]	233.8
speed [m/s]	70.2

Table 10: Calc. without wings: density: results

Calculations with wings

Std density:

Power [kW]	917.4
Flapping Angle [°]	1.71
Blade Tip Speed [m/s]	221
Speed [m/s]	66.6

Table 11: Calc. with wings: Std: results

Density (8000ft+dT):

Power [kW]	674.5
Flapping Angle [°]	2.5
Blade Tip Speed [m/s]	220
Speed [m/s]	66.1

Table 12: Calc. with wings: density: results